Contribution from the Department of Chemistry and Laboratory of Molecular Structure and Bonding, Texas A&M University, College Station, Texas 77843, and Department of Chemistry, Michigan State University, East Lansing, Michigan 48824

Synthesis and Characterization of a Complex with a Very Long Os–Os Triple Bond, $Os_2(DFM)_4Cl_2$

F. Albert Cotton,*[1a] Tong Ren,[1a] and Judith L. Eglin[1b]

Received December 4, 1990

A new compound that contains an Os_2^{6+} core bridged by four DFM anions (HDFM = di-*p*-tolylformamidine) has been prepared in 50% yield from the reaction of $Os_2(O_2CCH_3)_4Cl_2$ with molten HDFM and has been characterized by X-ray diffraction and magnetic susceptibility measurements from ca. 5 to ca. 300 K. Dark brown $Os_2(DFM)_4Cl_2 \cdot C_6H_6 \cdot C_6H_{14}$ crystallizes in the space group $P\bar{1}$ with a = 12.173 (7) Å, b = 14.533 (6) Å, c = 10.912 (2) Å, α = 93.15 (4)°, β = 103.56 (4)°, γ = 65.76 (3)°, V = 1709 (1) Å^3, and Z = 1. The molecule has Os–Os = 2.467 (1) Å, and an eclipsed ligand arrangement (averaged torsion angle of 0.1 (4) °). The magnetic susceptibility has been shown to have a temperature dependence consistent with the zero-field-splitting (ZFS) model as applied to ground-state configuration $(\sigma)^2(\pi)^4(\delta)^2(\pi^*)^2$. Because of the large spin–orbit coupling constant, the lowest state, which is nonmagnetic, lies ca. 1350 cm^{-1} below the lowest magnetic states.

Introduction

It is of primary importance in the chemistry of compounds with metal–metal bonds to understand the correlation between the molecular and the electronic structures.[2] Extensive study has been focused on this subject since the discovery of the metal–metal quadruple bond, with the emphasis on the dimers formed by the group 6 triad and Re. In the last three years significant progress has been made in the area of diruthenium chemistry, although it had been neglected for almost two decades. The electronic structures of $Ru^{II}_2(LL)_4L_2$[3] type complexes were elucidated in great detail from the analysis of structural, spectroscopic, and magnetic data, as well as MO calculations.[4-9] This success has naturally encouraged a similar effort to obtain detailed knowledge of the electronic structures of dinuclear osmium compounds.

The chemistry of $Os^{III}_2(LL)_4X_2$ type compounds is relatively new. The first such complex, $Os_2(hp)_4Cl_2$, was synthesized and structurally characterized in this laboratory in 1980.[10] The Os–Os distances in two differently solvated forms of this compound are 2.344 and 2.357 Å. Later, several $Os_2(O_2CR)_4Cl_2$ complexes were reported with Os–Os bond lengths of 2.301, 2.316, and 2.314 Å for the butyrate,[11] propionate,[12] and acetate[12] complexes, respectively. A third pertinent type of complex is $Os_2(PhCONH)_4X_2$,[13] with Os–Os distances of 2.367 Å for X = Cl and 2.384 Å for X = Br. Since Os_2^{6+} is a d^5–d^5 system, a triple bond is naturally expected for these compounds. The electronic structures beyond $(\sigma)^2(\pi)^4(\delta)^2$, by analogy to the previously discussed diruthenium(II,II) system,[5,7,8] can be one of three configurations, $(\delta^*)^2$, $(\delta^*)(\pi^*)$, and $(\pi^*)^2$. It is notable that all the Os–Os distances just mentioned are at least 0.1 Å longer than those observed for the diamagnetic $Os_2X_8^{2-}$ (X = Cl, Br, and I) species,[14] which definitely belong to the $(\delta^*)^2$ category. Another important fact is that all $Os^{III}_2(LL)_4X_2$ compounds mentioned above have temperature-dependent effective magnetic moments that range from 2.00 to 1.6 μ_B at room temperature and decrease at lower temperature. On the basis of these observations, it was postulated that the ground-state configuration is $(\delta^*)^2$ but that this is in thermal equilibrium with a low-lying triplet state derived from an excited configuration, either $(\delta^*)(\pi^*)$ or $(\pi^*)^2$, to give an appreciable room-temperature paramagnetism. Obviously, to clarify this problem, more detailed magnetic and spectroscopic study of these known complexes will be necessary.

In the meantime, we note that for the diruthenium(II,II) system the replacement of the carboxylate ligands by much more basic ligands, such as triazenido or diformamidino, alters the electronic structure dramatically because of the large increase in the π basicity.[4-6,8,9] It was also of interest to see how the electronic structure of diosmium systems would respond to a similar substitution.

Experimental Section

The preparations and purifications were carried out under argon in standard Schlenkware. $Os_2(OAc)_4Cl_2$ was synthesized by refluxing $[OsCl_6]^{2-}$ with acetic acid in air according to the literature.[11] Di-*p*-tolyldiformamidine (HDFM) was synthesized through high-temperature condensation between *p*-toluidine and triethyl orthoformate.[15] All solvents were freshly distilled under N_2 with suitable drying reagents.

Preparation of $Os_2(DFM)_4Cl_2$. A 0.136-g amount of $Os_2(OAc)_4Cl_2$ (0.2 mmol) and 0.45 g of di-*p*-tolyldiformamidine (2 mmol) were well mixed, and then the mixture was heated at 140 °C for about 1 h. The brown mixture turned black with some colorless oily liquid being evolved. The reaction mixture was washed with 2 × 10 mL of hexane, and then the desired complex was extracted with 10 mL of benzene. The benzene extract still contained a substantial amount of unreacted ligand, which was then largely removed by sublimation under vacuum. The product was finally purified by recrystallization from a large volume of hot hexane, resulting in a dark brown-purple microcrystalline material. The yield was usually around 50%. Reaction of the acetate with the lithium salt of the ligand was not a useful one, as it resulted in a dark purple mixture that was hard to purify and characterize. The purified solid sample is air stable. Crystals of X-ray quality were deposited as a result of layering a benzene extract with hexane.

^{1}H NMR ($CDCl_3$): 6.8–7.1 ppm (m, aromatic protons), 2.3 ppm (s, CH_3). UV–vis (C_6H_6): 496, 419 nm.

Physical Measurements. The UV–visible spectra were measured on a Cary 17D spectrometer at ambient temperature using glass cells (900–400 nm) and quartz cells (400–220 nm). ^{1}H NMR spectra were recorded on a Varian-200 spectrometer at ambient temperature. Room-temperature magnetic susceptibilities were determined on a MSB 1 (Johnson Matthey) magnetic susceptibility balance (calibrated with $HgCo(SCN)_4$). The cyclic voltammetry (CV) measurements were performed on a BAS 100 electrochemical analyzer, in 0.1 M (*n*-

(1) (a) Texas A&M University (b) Michigan State University. Present address: Texas A&M University.
(2) (a) Cotton, F. A.; Walton, R. A. *Multiple Bonds Between Metal Atoms*; John Wiley & Sons, New York, 1982. (b) Cotton, F. A.; Walton, R. A. *Struct. Bonding* **1985**, *62*.
(3) LL is an abbreviation for any three-atom, uninegative, bridging bidentate ligand; X is a uninegative monodentate axial ligand.
(4) Lindsay, A. J.; Wilkinson, G.; Motevalli, M.; Hursthouse, M. B. *J. Chem. Soc., Dalton Trans.* **1987**, 2723.
(5) Cotton, F. A.; Matusz, M. *J. Am. Chem. Soc.* **1988**, *110*, 5761.
(6) Cotton, F. A.; Feng, X. *Inorg. Chem.* **1989**, *28*, 1180.
(7) Cotton, F. A.; Miskowski, V. M.; Zhong, B. *J. Am. Chem. Soc.* **1989**, *111*, 6177.
(8) (a) Cotton, F. A.; Ren, T.; Eglin, J. L. *J. Am. Chem. Soc.* **1990**, *112*, 3439. (b) Cotton, F. A.; Ren, T.; Eglin, J. L. *Inorg. Chem.*, preceding paper in this issue.
(9) Cotton, F. A.; Ren, T. Manuscript in Preparation.
(10) Cotton, F. A.; Thompson, J. L. *J. Am. Chem. Soc.* **1980**, *102*, 6437.
(11) Behling, T.; Wilkinson, G.; Stephenson, T. A.; Tocher, D. A.; Walkinshaw, M. D. *J. Chem. Soc., Dalton Trans.* **1983**, 2109.
(12) Cotton, F. A.; Chakravarty, A. R.; Tocher, D. A. *Inorg. Chim. Acta* **1984**, *87*, 115.
(13) Chakravarty, A. R.; Cotton, F. A.; Tocher, D. A. *Inorg. Chem.* **1985**, *24*, 1334.
(14) Cotton, F. A.; Vidyasagar, K. *Inorg. Chem.* **1990**, *29*, 3197 and earlier references therein.
(15) Bradley, W.; Wright, I. *J. Chem. Soc.* **1956**, 640.

0020-1669/91/1330-2559$02.50/0

Table I. Crystallographic Parameters for $Os_2(DFM)_4Cl_2 \cdot C_6H_6 \cdot C_6H_{14}$

chem formula	$Os_2Cl_2N_8C_{72}N_{80}$
fw	1508.8
space group	$P\bar{1}$ (No. 2)
a, Å	12.173 (7)
b, Å	14.533 (6)
c, Å	10.912 (2)
α, deg	93.15 (4)
β, deg	103.56 (4)
γ, deg	65.76 (3)
V, Å^3	1709 (1)
Z	1
d_{calc}, g cm^{-3}	1.466
μ, cm^{-1}	38.4
λ(Mo Kα), Å	0.71073
data collcn instrument	Rigaku AFC5R
T, °C	20 ● 1
R^a	0.052
R_w^b	0.067

$^a R = \sum||F_o| - |F_c||/\sum|F_o|$. $^b R_w = [\sum w(|F_o| - |F_c|)^2/\sum w|F_o|^2]^{1/2}$; $w = 1/\sigma^2(|F_o|)$.

Bu)$_4$NBF$_4$/CH$_2$Cl$_2$ solution at a Pt electrode, with the reference electrode Ag/AgCl. Ferrocene was oxidized at +450 mV under the experimental conditions.

The variable-temperature magnetic susceptibility data were measured with an SHE 800 Series SQUID (superconducting quantum interference device) magnetometer at Michigan State University over a temperature range of 1.2 to 300 K in applied fields of 5 and 7 kG. The sample was rapidly cooled from room temperature to 5 K in zero field by loading it directly into the susceptometer and also slowly cooled from 300 to 5 K in a field of 5 kG. No field dependence was observed or any difference in the susceptibility due to the two different thermal treatments of the sample done at 5 kG. The sample used was vacuum-dried at 80 °C overnight and, hence, is assumed to be solvent-free.

X-ray Crystallography. A purple plate was mounted under a mixture of mineral oil and the mother liquid in a Lindemann capillary. Indexing based on 13 reflections with 2θ ranging from 15 to 19° gave a triclinic cell. The data were collected on a Rigaku AFC5R diffractometer via an ω-scan method due to the broad peak profiles observed during the indexing (widths of the reflections for indexing were between 1.40 and 1.65°). The normal crystallographic procedures presented elsewhere[16,17] were applied. The data were corrected for decay (overall 0.9%), Lorentz, and polarization effects. No absorption corrections were applied to the data set.

The Patterson method was used to locate the osmium atom, which was then refined isotropically to a low residual. The other non-hydrogen atoms in the molecule were then located and refined in the normal way. After the anisotropic refinement of these atoms converged, a difference Fourier map revealed peaks indicating the existence of a benzene molecule at an inversion center as well as a three-peak zigzag chain with one of the terminal atoms close to another inversion center. The benzene molecule was refined with isotropic thermal parameters to an ideal shape. The three-peak chain was refined as a half of a hexane molecule, which was converged with a 1.9-Å distance between the terminal carbon and its inversion image. Since the quality of the data was insufficient, no further efforts to conduct restricted refinement were made. For the same reason none of the hydrogen atoms were introduced. The results of the crystallographic procedures are summarized in Table I. The positional parameters are listed in Table II.

Computational Procedures. The SCF-MS (multiple scattering)-Xα method[18] was used to calculate the electronic structure. In the calculation Norman's overlapping atomic sphere radii[19] were assumed to be 88.5% of the atomic number radii. The outer sphere was made tangent to the outer atomic spheres. The α values of the atoms were adopted from Schwartz,[20] and the one for both intersphere and outersphere was taken as the valence-electron-weighted average of the atomic α. The SCF iteration was considered to be converged when the potential change was less than 10^{-3} Ry. Only spin-restricted SCF was applied. The relativistic correction was introduced after the normal SCF calculation had converged.

$Os_2(HNCHNH)_4Cl_2$ was employed as the model complex, where the DFM anion of the compound is replaced with $[HNCHNH]^-$. The model was idealized to D_{4h} symmetry, with the following averaged bond lengths and angles: Os–Os = 2.467 Å, Os–Cl = 2.478 Å, Os–N = 2.061 Å, N–C = 1.325 Å, Os–Os–N = 88°, Os–N–C = 120°. The C–H and N–H bond lengths were assumed to be 1.10 and 1.00 Å, respectively.

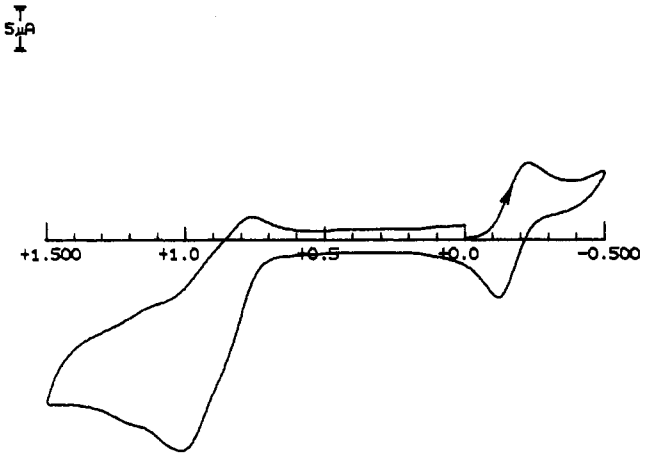

Figure 1. Cyclic voltammogram of $Os_2(DFM)_4Cl_2$ (scan speed 200 mV/s).

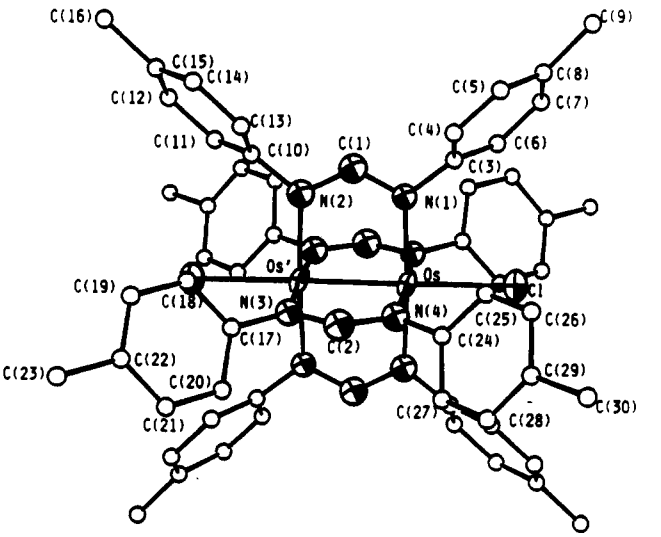

Figure 2. ORTEP drawing of $Os_2(DFM)_4Cl_2$.

Results and Discussion

The synthesis was carried out by using a molten reaction similar to those used for $Ru_2(xhp)_4$:[8]

$$Os_2(OAc)_4Cl_2 + 4HDFM \rightarrow Os_2(DFM)_4Cl_2 + 4HOAc\uparrow \quad (1)$$

The equilibrium is driven to the right at high temperatures due to the volatility of HOAc. The yield from the above molten reaction should have been quantitative. However, the isolated yield of the purified compound was limited by its extreme solubility in most organic solvents. Synthesis via the use of LiDFM (the route for $Ru_2(DFM)_4$[9] and $Ru_2(p\text{-tolNNN}p\text{-tol})_4$[5]) was not successful. This is an indication that the acetate ligand of $Os_2(OAc)_4Cl_2$ is less labile than that of $Ru_2(OAc)_4$. Also it is possible

(16) Bino, A.; Cotton, F. A.; Fanwick, P. E. *Inorg. Chem.* **1979**, *18*, 3558.
(17) Cotton, F. A.; Frenz, B. A.; Deganello, G.; Shaver, A. *J. Organomet. Chem.* **1973**, *50*, 227.
(18) (a) Slater, J. C. *Quantum Theory of Molecules and Solids*; McGraw-Hill: New York, 1974. (b) Johnson, K. H. *Adv. Quantum Chem.* **1973**, *7*, 143. (c) Connolly, J. W. D. In *Semiempirical Methods of Electronic Structure Calculation. Part A: Techniques*; Segal, G. A., Ed.; Plenum Press: New York, 1977. (d) A version of the SCF-Xα program package by M. Cook (Harvard) and B. E. Bursten and G. G. Stanley (Texas A&M University) using relativistic mass-velocity and Darwin corrections developed by Wood and Boring (Wood, J. H.; Boring, M. A. *Phys. Rev. B: Condens. Matter* **1978**, *18*, 2701) was used.
(19) Norman, J. G., Jr. *Mol. Phys.* **1976**, *31*, 1191.
(20) Schwartz, K. *Phys. Rev.* **1972**, *5*, 2466.

Table II. Positional Parameters and Their Estimated Standard Deviations for $Os_2(DFM)_4Cl_2 \cdot C_6H_6 \cdot C_6H_{14}$

atom	x	y	z	B,[a] Å^2
Os	−0.05330 (4)	0.08470 (3)	−0.05343 (4)	2.174 (9)
Cl	−0.1592 (3)	0.2565 (2)	−0.1564 (3)	3.53 (8)
N(1)	0.0511 (8)	0.1331 (6)	0.0909 (8)	2.3 (2)
N(2)	0.1519 (8)	−0.0277 (7)	0.1916 (9)	2.8 (2)
N(3)	−0.1861 (8)	0.1175 (7)	0.0495 (8)	2.4 (2)
N(4)	−0.0839 (8)	−0.0437 (7)	0.1511 (9)	2.8 (2)
C(1)	0.132 (1)	0.0694 (8)	0.183 (1)	2.9 (3)
C(2)	−0.175 (1)	0.0480 (9)	0.132 (1)	3.2 (3)
C(3)	0.051 (1)	0.2325 (9)	0.102 (1)	3.0 (3)
C(4)	0.164 (1)	0.2413 (9)	0.109 (1)	3.2 (3)
C(5)	0.171 (1)	0.3335 (9)	0.134 (1)	3.6 (3)
C(6)	−0.051 (1)	0.316 (1)	0.122 (1)	3.7 (3)
C(7)	−0.042 (1)	0.4073 (9)	0.146 (1)	4.1 (4)
C(8)	0.069 (1)	0.417 (1)	0.156 (1)	4.2 (4)
C(9)	0.078 (2)	0.517 (1)	0.186 (2)	5.7 (4)
C(10)	0.249 (1)	−0.0794 (8)	0.297 (1)	3.0 (3)
C(11)	0.227 (1)	−0.1309 (9)	0.390 (1)	3.5 (3)
C(12)	0.324 (1)	−0.177 (1)	0.497 (1)	4.2 (4)
C(13)	0.365 (1)	−0.0776 (9)	0.311 (1)	3.9 (3)
C(14)	0.460 (1)	−0.124 (1)	0.420 (1)	5.1 (4)
C(15)	0.440 (1)	−0.175 (1)	0.511 (1)	5.2 (4)
C(16)	0.543 (2)	−0.224 (2)	0.629 (2)	8.5 (6)
C(17)	−0.291 (1)	0.2112 (9)	0.048 (1)	3.1 (3)
C(18)	−0.385 (1)	0.248 (1)	−0.060 (1)	4.7 (4)
C(19)	−0.493 (1)	0.333 (1)	−0.055 (2)	5.0 (4)
C(20)	−0.304 (1)	0.260 (1)	0.163 (1)	4.0 (3)
C(21)	−0.410 (1)	0.346 (1)	0.167 (1)	5.2 (4)
C(22)	−0.509 (1)	0.382 (1)	0.058 (2)	5.5 (4)
C(23)	−0.627 (1)	0.473 (1)	0.065 (2)	7.1 (5)
C(24)	−0.094 (1)	−0.1020 (8)	0.247 (1)	2.7 (3)
C(25)	−0.107 (1)	−0.1912 (9)	0.220 (1)	3.7 (3)
C(26)	−0.128 (1)	−0.242 (1)	0.310 (1)	4.0 (3)
C(27)	−0.096 (1)	−0.064 (1)	0.368 (1)	3.8 (3)
C(28)	−0.117 (1)	−0.116 (1)	0.458 (1)	4.9 (4)
C(29)	−0.133 (1)	−0.204 (1)	0.428 (1)	4.5 (4)
C(30)	−0.156 (1)	−0.265 (1)	0.528 (1)	6.2 (4)
C(31)	0.552 (2)	1.003 (2)	0.128 (2)	9.5 (6)*
C(32)	0.558 (2)	0.913 (1)	0.075 (2)	7.6 (5)*
C(33)	0.489 (2)	1.093 (1)	0.048 (2)	8.1 (5)*
C(34)	0.447 (3)	0.550 (2)	0.434 (3)	14 (1)*
C(35)	0.323 (3)	0.563 (2)	0.455 (3)	15 (1)*
C(36)	0.210 (3)	0.581 (3)	0.540 (3)	16 (1)*

[a] Starred B values are for atoms that were refined isotropically. B values for anisotropically refined atoms are given in the form of the equivalent isotropic displacement parameter defined as $(4/3)[a^2\beta_{11} + b^2\beta_{22} + c^2\beta_{33} + ab(\cos\gamma)\beta_{12} + ac(\cos\beta)\beta_{13} + bc(\cos\alpha)\beta_{23}]$.

that the lithium salt not only reacts to replace the bridging acetates but also the axial chlorides. $Os_2(DFM)_4Cl_2$, similarly to $Os_2(OAc)_4Cl_2$,[11] undergoes a quasi-reversible reduction at −174 mV and an irreversible oxidation at +1050 mV, as shown by the CV study (Figure 1). The former suggests there could be a stable $Os_2(DFM)_4Cl_2^-$ species, while the later indicates a cleavage of the Os–Os bond upon the oxidation, perhaps due to high formal charge on the metal core.

An ORTEP drawing of the molecule is presented in Figure 2, and selected bond lengths and angles are listed in Table III. The ligands are arranged in an effectively eclipsed geometry, with a mean torsion angle of 0° because of the inversion center between the osmium atoms. The torsion angles N(1)–Os–Os′–N(2) and N(4)–Os–Os′–N(3) are 0.05 (35) and 0.13 (0.37)°, respectively, all smaller than 1σ. This is consistent with the δ^* orbital being empty and hence the full retention of a metal–metal δ bond. The Os–Os distance (2.467 (1) Å) is 0.100 Å longer than the previously known longest Os–Os distance, 2.367 (3) Å in $Os_2(PhCONH)_4Cl_2$,[13] among all known $Os_2(LL)_4Cl_2$ type complexes. The average Os–N and N–C_b (C_b is the central bridging carbon in the ligand) distances are equivalent (within the 3σ range) to those found in the $Ru_2(DFM)_4$ study.[9] The structure of the ligand is thus essentially insensitive to the change of the metal center. The spacing between two nitrogen atoms on the same ligand is about 2.35 Å, which is longer than those found for $Mo_2(DFM)_4$ (2.21 Å), $Mo_2(DFM)_4^+$ (2.31 Å),[21] and $Ru_2(DFM)_4$ (2.32 Å).

Table III. Selected Bond Distances (Å) and Angles (deg) for $Os_2(DFM)_4Cl_2 \cdot C_6H_6 \cdot C_6H_{14}$[a]

Bond Distances			
Os–Os	2.4672 (6)	Os–N(4)	2.056 (10)
Os–Cl	2.478 (3)	N(1)–C(1)	1.313 (12)
Os–N(1)	2.065 (9)	N(2)–C(1)	1.33 (2)
Os–N(2)	2.057 (10)	N(3)–C(2)	1.33 (2)
Os–N(3)	2.065 (10)	N(4)–C(2)	1.326 (12)

Bond Angles			
Os–Os–Cl	178.76 (8)	Os–N(1)–C(1)	120.1 (8)
Os–Os–N(1)	87.9 (2)	Os–N(2)–C(1)	119.4 (7)
Os–Os–N(2)	88.5 (2)	Os–N(3)–C(2)	119.4 (7)
Os–Os–N(3)	88.3 (2)	Os–N(4)–C(2)	119.9 (9)
Os–Os–N(4)	88.3 (3)	N(1)–C(1)–N(2)	124 (1)
N(1)–Os–N(2)	176.4 (3)	N(3)–C(2)–N(4)	124 (1)
N(3)–Os–N(4)	176.7 (3)		

[a] Numbers in parentheses are estimated standard deviations in the least significant digits.

The flexibility of the DFM^- ligand geometry indicates that the Os–Os distance is determined mainly by the electronic structure rather than by the geometrical requirements of the ligand.

The ^1H NMR spectrum of this complex contained the resonances for both CH_3 and the aromatic protons in the normal region and with normal sharpness. A magnetic susceptibility measurement at room temperature (Faraday balance) showed that $\chi_M \approx 0$, which means the paramagnetism of the molecule is essentially canceled by the diamagnetic contribution from the closed-shell electrons. Hence $\chi_{para} \approx -\chi_{dia} = 0.000\,662$ emu, which corresponds to a magnetic moment (μ_{eff}) of ca. 1.2 μ_B. The origin of this weak paramagnetism is localized at the metal core, since there is no apparent paramagnetic shifting in the proton NMR spectrum of the tolyl group.

As we pointed out in the beginning, there are three possible configurations of the highest two electrons for diosmium(III,III) complexes, i.e., $(\delta^*)^2$, $(\pi^*)(\delta^*)$, and $(\pi^*)^2$. The second configuration was shown to be very paramagnetic over the entire temperature region (0–300 K), since the first-order spin–orbit coupling should result in a spin doublet ($M_S = \pm 1$) as the ground state.[8b] Hence it can be eliminated as a possible ground-state configuration. The $(\delta^*)^2$ configuration, when in thermal equilibrium with a low-lying excited-state configuration, for example, $(\pi^*)(\delta^*)$, could result in weak paramagnetism at room temperature. It should, however, also give a very short Os–Os distance, which is obviously contrary to the observed bond distance.

On the other hand, the $(\pi^*)^2$ configuration is consistent with the very long Os–Os bond length. As shown by the studies of the carboxylate[7] and hydroxypyridinate[8] complexes of diruthenium, the ground-state term for such a configuration is a spin-triplet and orbit-singlet, which is further split by second-order spin–orbit coupling into a singlet ($M_S = 0$) and a doublet ($M_S = \pm 1$). The singlet lies lowest with the result that there is paramagnetism described by the following molar susceptibility equation:

$$\chi = \frac{2Ng_{eff}^2\mu_B^2}{3k_BT}\,\frac{e^{-x} + \frac{2}{x}(1 - e^{-x})}{1 + 2e^{-x}} \qquad (2)$$

where k_B is the Boltzmann constant, N is Avogadro's number, T is the temperature in Kelvin, $x = D/k_BT$, and D is the zero field splitting (ZFS) caused by second-order spin–orbit coupling. It is noteworthy that the room-temperature paramagnetism here is much lower than those observed for the diruthenium(II,II) complexes. However, it is well-known that high-spin monomeric osmium complexes often display only weak paramagnetism due to the large spin–orbit coupling effect.[22-24] The value of ξ can be estimated from these experiments to be in the range 3600–8000

(21) Cotton, F. A.; Feng, X.; Matusz, M. *Inorg. Chem.* **1989**, *28*, 594.
(22) Abragam, A.; Bleaney, B. *Electron Paramagnetic Resonance of Transition Ions*; Oxford University Press: Oxford, England, 1970.
(23) Kamimura, H.; Koide, S.; Sekiyama, H.; Sugano, S. *J. Phys. Soc. Jpn.* **1960**, *15*, 1264.
(24) Greenslade, D. J.; Stevens, K. W. H. *Proc. Phys. Soc.* **1967**, *91*, 627.

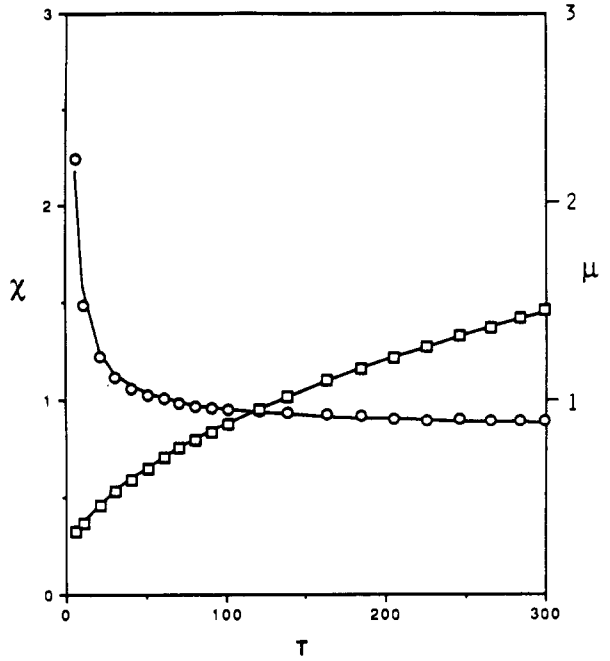

Figure 3. Magnetic susceptibility χ ($\times 10^{-3}$ cgs) and magnetic moments μ (μ_B) vs T (K) for $Os_2(DFM)_4Cl_2$, where (O) gives the measured χ and the solid line overlapped with (O) is calculated according to eq 2. The squares and the solid line overlapped with them are the measured and simulated magnetic moments, respectively, with the scale on the right side.

cm^{-1} as compared to ca. 1000 cm^{-1} for Ru^{II}, and the weak paramagnetism of our dimer could also be attributed to this effect. In fact it can be shown that the ZFS for a $(\pi^*)^2$ configuration is given by the following expression:[25]

$$D = \frac{\xi^2}{4\Delta E_{ST}} \qquad (3)$$

where ΔE_{ST} is the singlet–triplet separation. Comparing the ξ value of Os to that of Ru, we would naturally expect very weak paramagnetism at room temperature. The D value, the separation between the nonmagnetic state and the lowest magnetic states of the Os complex, should be almost 10 times of that in the $Ru_2(xhp)_4$ case, i.e., ca. 2400 cm^{-1}.

To provide further evidence for a $(\pi^*)^2$ ground-state configuration, variable-temperature (5–300 K) magnetic susceptibility data were measured and simulated according to eq 2. Both the measured and simulated susceptibilities as well as the corresponding effective magnetic moments, μ_{eff}, are plotted in Figure 3. A simple Curie type magnetic impurity with $S = {}^3/_2$ was assumed to be present as a contaminant in the bulk sample to explain the fast rising tail in the low-temperature region. The parameters obtained from the simulation, as defined before,[7,8] are $\alpha = 0.6\%$, $D = 1350$ cm^{-1}, and $g_{av} = 1.802$. From the plot shown in Figure 3, it is clear that the measured data and the model simulation match well. Here we also note that the D value determined experimentally is somewhat smaller than the one expected from the comparison of ξ values. One possible explanation for this is that the lowest $M_S = \pm 1$ states are not from $^3A_{2g}$ but from ^3E_u ($(\pi^*)(\delta^*)$ configuration). Since the van Vleck equation does not contain any information about the symmetry property of the states, further spectroscopic study is necessary to completely resolve this problem. It is also possible that the large ligand contribution to both π^* and δ^* orbitals (see the Xα results below) results in the reduction of the D value.

An Xα calculation with a relativistic correction was carried out with the model compound $Os_2(HNCHNH)_4Cl_2$. The validity of the substitution of $HNCHNH^-$ for DFM^- has been established in previous studies of DFM complexes of Rh[6] and Mo.[21] The

(25) Ren, T. Ph.D. Dissertation, Texas A&M University, 1990.

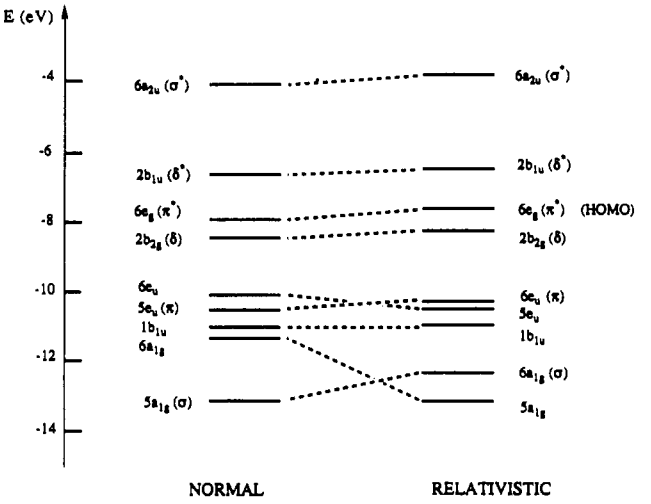

Figure 4. Effect of relativistic correction on metal–metal bonding (antibonding) orbitals.

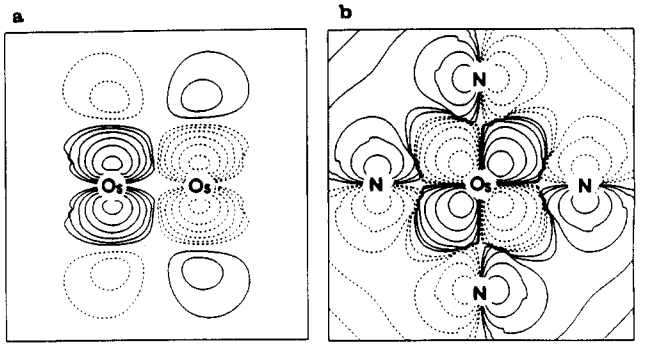

Figure 5. δ^* of $Os_2(HNC(H)NH)_4Cl_2$: (a) projection plane bisects the xz and yz planes; (b) projection plane is parallel to the xy plane and contains one Os atom.

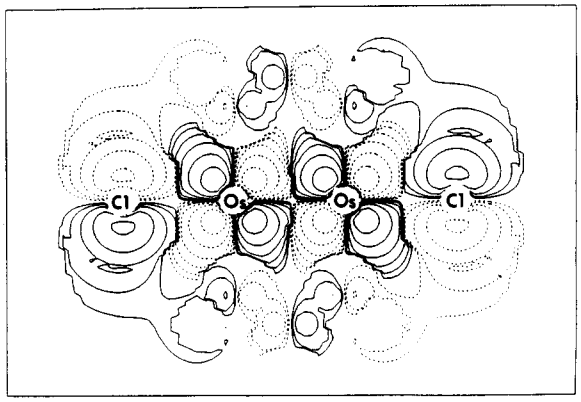

Figure 6. π^* of $Os_2(HNC(H)NH)_4Cl_2$. The projection plane is the xz plane.

energy levels and the populations of upper valence MOs from the converged SCF iteration are listed in Table IV. The orbitals omitted from the table are 20 (5 e-type) low-lying valence orbitals that basically consist of all C–N, C–H, and N–H σ-bonding orbitals as well as the four lowest delocalized N–C–N π-bonding orbitals. They have no direct relevance to our discussion.

To illustrate the influence of the relativistic effect, all the molecular orbitals from both the normal and corrected calculation with metal character above 50% are plotted in Figure 4. It should be noted that the labels for metal–metal π-bonding and σ-bonding orbitals are different due to the level crossing after the correction. To make clear why this is so, two additional energy levels that have mainly ligand character have been added in each case ($6e_u$ and $6a_{1g}$ in the normal calculation and $5e_u$ and $5a_{1g}$ in the relativistic calculation). As can be seen, the energies of all the orbitals dominated by metal character are lifted by the relativistic cor-

Table IV. Upper Valence Molecular Orbitals for $Os_2(HNC(H)NH)_4Cl_2$[a]

level	E, eV	% charge						Os angular contribution
		Os	Cl	N	C	Hc	Hn	
$6a_{2u}$	−3.869	72	18	9	0	0	1	1% s, 1% p, 98% d
$2b_{1u}$	−6.598	56	0	44	0	0	0	100% d
$6e_g$	−7.725	83	15	0	1	0	1	100% d
$1a_{1u}$	−7.958	0	0	100	0	0	0	
$7a_{1g}$	−8.112	31	66	1	1	0	0	12% s, 31% p, 57% d
$2b_{2g}$	−8.369	76	0	9	15	0	0	100% d
$5e_g$	−8.426	0	1	99	0	0	0	
$7e_u$	−8.881	25	71	3	0	0	1	100% d
$4e_g$	−9.587	15	82	2	1	0	0	100% d
$6e_u$	−10.371	58	26	10	1	1	3	2% p, 98% d
$5a_{2u}$	−10.446	21	79	0	0	0	0	16% s, 17% p, 67% d
$5e_u$	−10.530	19	0	55	16	9	2	28% p, 72% d
$1a_{2g}$	−10.901	0	0	69	31	0	0	
$1b_{1u}$	−11.057	56	0	44	0	0	0	100% d
$4e_u$	−11.604	6	0	64	25	4	1	
$3e_g$	−12.280	9	0	79	2	0	10	
$6a_{1g}$	−12.460	57	30	6	3	4	1	39% s, 1% p, 60% d
$1b_{2g}$	−12.742	28	0	55	17	0	0	100% d
$5a_{1g}$	−13.225	33	2	26	17	18	4	9% s, 1% p, 90% d
$4b_{1g}$	−13.331	30	0	27	20	20	4	100% d
$4a_{2u}$	−14.986	25	0	59	0	0	16	49% s, 51% d
$3b_{2u}$	−15.089	33	0	53	0	0	14	100% d

[a] % charge indicates relative amount of charge in the atomic spheres, and metal angular contribution is given only when >10%. The gap is between the LUMO and the HOMO.

rection, while the levels of the ligand-based orbitals are lowered. This is consistent with the trend observed for the relativistic $X\alpha$ calculation of $Re_2Cl_8^{2-}$.[26]

The molecular orbitals listed in Table IV can be roughly divided into three groups: the metal–metal bonding and antibonding orbitals which have more than 55% metal contributions, the metal–ligand bonding orbitals, which have about 30% or less metal characters, and the ligand-localized π-type orbitals. The predominant metal–metal bonding and antibonding orbitals are (in descending order of energy) $6a_{2u}$ (σ^*), $2b_{1u}$ (δ^*, LUMO), $6e_g$ (π^*, HOMO), $2b_{2g}$ (δ), $6e_u$ (π), and $6a_{1g}$ (σ) with the HOMO being half-occupied. The most important result of this calculation is that because of the perturbation by the ligands the δ^* orbital lies above the π^* orbital with a fairly large separation of 1.13 eV, thus leading clearly to a $(\pi^*)^2$ configuration. An effective triple bond between the osmium centers is therefore established. The large δ^*–π^* separation, as we expected from the studies of $Ru_2(tolNNNtol)_4$[6] and $Ru_2(DFM)_4$,[9] is due to the strong π basicity of DFM^-.

Some other new features of the electronic structures are also revealed by the results of this calculation. For Os(III) the d-orbital energy is lower than that of Ru(II) due to the higher effective nuclear charge. The δ^* orbital now should be better matched with the ψ_1 of the nitrogen, so a strong interaction now exists, as shown by the contour plot of the δ^* orbital in Figure 5, especially part b. This interaction helps to enlarge the LUMO–HOMO separation. Although the charge contribution of the nitrogen atoms to the δ^* orbital (44%) for $Os_2(DFM)_4Cl_2$ is substantially larger than that found for $Ru_2(DFM)_4$ (33%),[9] the separation is still about the same. The explanation is simply that the π^* orbital of the metal core is interacting (antibonding) with the lone pair of the axial Cl atoms, which results in the 15% contribution in $6e_g$ (π^* orbital of the M–M bond) from two Cl atoms. Hence the shift of the δ^* orbital is canceled by the shift of the π^* orbital. The antibonding interaction between the axial chlorine atom and the osmium atom is clearly evident in the contour plot of the π^* orbital (Figure 6).

The electronic absorption spectrum of $Os_2(DFM)_4Cl_2$ contains two peaks at 496 and 419 nm. The lowest energy transition, according to above discussion of the electronic structure, should be π^* (HOMO) → δ^* (LUMO), which is (x,y)-polarized in D_{4h} point symmetry. Taking into account that the δ^* energy could be underestimated and that actual state-to-state energy difference is always larger than the difference between the single electron energy levels, we assign the transition at 496 nm (2.5 eV) as $\pi^* \rightarrow \delta^*$ ($^1A_{1g} \rightarrow {}^1E_u$), although the calculated orbital separation is only 1.13 eV. The other transition (419 nm (3.0 eV)) is assigned as $\delta \rightarrow \delta^*$ ($^1A_{1g} \rightarrow {}^1A_{2u}$, z-polarized), while the calculated value (1.77 eV) is, as always, much lower due to the inadequate inclusion of correlation effects in the Hartree–Fock formulation.[2]

(26) Bursten, B. E.; Cotton, F. A.; Fanwick, P. E.; Stanley, G. G. *J. Am. Chem. Soc.* **1983**, *105*, 3082.

Conclusions

In this work the ground-state electronic structure of $Os_2(DFM)_4Cl_2$ has been firmly established by molecular structural, theoretical, and magnetic studies. This is the first example of an $Os_2(LL)_4X_2$ type compound that has been fully characterized in all three respects. The π-basicity model, initially suggested for diruthenium(II,II) complexes, is shown to be applicable to diosmium(III,III) as well. It is notable that in comparison with Ru(II,II), the valence d-orbital energy of Os(III) is substantially downshifted due to the higher nuclear charge, which means that the d orbitals are *generally* better matched with the frontier orbitals of LL^- type ligands. Therefore, it is *possible* that some other diosmium(III,III) complexes also have the δ^* and π^* in the order $\pi^* < \delta^*$, by at least a small amount. We hope that magnetic data and suitable model SCF calculations will reveal the correct electronic structures of other $Os_2(LL)_4X_2$ in the near future.

In all previously studied $Os_2(LL)_4X_2$ compounds, where LL^- has been RCO_2^-, hp^-, or $PhCONH^-$, the Os–Os distances have been in the range 2.30–2.38 Å and the magnetic properties have suggested that the structures determined were those of molecules with $(\delta^*)^2$ configurations partly mixed with some having the $(\delta^*)(\pi^*)$ configuration. Thus, we can conclude that the bond length change caused by the shift of one electron from a δ^* to a π^* orbital is about +0.07 Å, in accord with the weakly and strongly antibonding characters of the δ^* and π^* orbitals, respectively.

Acknowledgment. We thank the National Science Foundation for support. We thank Professor J. L. Dye of Michigan State University for making his SQUID facility available for the measurement of the susceptibility data and Drs. X. Feng and L. R. Falvello of this laboratory for the helpful discussions.

Supplementary Material Available: Complete tables of crystal data, bond distances and angles, anisotropic displacement parameters, and magnetic susceptibility data and a full table of the valence molecular orbitals (9 pages); a table of observed and calculated structure factors (19 pages). Ordering information is given on any current masthead page.